Chinese Journal of Oceanology and Limnology
Vol. 31 No. 3, P. 656-664, 2013
**http://dx.doi.org/10.1007/s00343-013-2169-0**

# Geostrophic meridional transport in tropical Northwest Pacific based on Argo profiles*

ZHANG Zhichun (张志春)[1, 2, 3], YUAN Dongliang (袁东亮)[1, 2, **], Peter C. CHU[4]

[1] *Institute of Oceanology, Chinese Academy of Sciences, Qingdao 266071, China*

[2] *Key Laboratory of Ocean Circulation and Waves, Chinese Academy of Sciences, Qingdao 266071, China*

[3] *Graduate University of Chinese Academy of Sciences, Beijing 100049, China*

[4] *Naval Ocean Analysis and Prediction (NOAP) Laboratory, Department of Oceanography, Naval Postgraduate School, Monterey, California, USA*

Received Jul. 11, 2012; accepted in principle Sep. 10, 2012; accepted for publication Jan. 4, 2013


**Abstract** Absolute geostrophic currents in the North Pacific Ocean were calculated using P-vector method from newly gridded Argo profiling float data collected during 2004–2009. The meridional volume transport of geostrophic currents differed significantly from the classical Sverdrup balance, with differences of $10\times10^6$–$20\times10^6$ $m^3/s$ in the interior tropical Northwest Pacific Ocean. Analyses showed that errors of wind stress estimation could not explain all of the differences. The largest differences were found in the areas immediately north and south of the bifurcation latitude of the North Equatorial Current west of the dateline, and in the recirculation area of the Kuroshio and its extension, where nonlinear eddy activities were robust. Comparison of the geostrophic meridional transport and the wind-driven Sverdrup meridional transport in a high-resolution OFES simulation showed that nonlinear effects of the ocean circulation were the most likely reason for the differences. It is therefore suggested that the linear, steady wind-driven dynamics of the Sverdrup theory cannot completely explain the meridional transport of the interior circulation of the tropical Northwest Pacific Ocean.

**Keyword**: Sverdrup theory; absolute geostrophic current; P-vector

## 1 INTRODUCTION

The development of contemporary ocean circulation theory began with the pioneering work of Sverdrup (1947), and still regarded as one of the cornerstones of research on general ocean circulation dynamics. Much of the modern theory is built directly on this work. The Sverdrup theory assumes a linear dynamic framework, and proposes a dynamic balance called the Sverdrup balance, whereby the meridional transport of wind-driven ocean circulation can be obtained by integrating wind-stress curl without the need for detailed information on oceanic baroclinicity (Sverdrup, 1947).

To date, only a few studies have attempted to verify the accuracy of this theory (Leetmaa et al., 1977; Wunsch and Roemmich, 1985; Böning et al., 1991; Schmitz et al., 1992). Results of these studies have shown that the Sverdrup meridional transport is generally consistent with the meridional transport calculated directly from geostrophic currents based on hydrographic data in the northeastern subtropical North Atlantic Ocean. However, it is inconsistent with geostrophic transport in the northwestern subtropical North Atlantic Ocean. The difference has been attributed to buoyancy-forced meridional overturning circulation in the North Atlantic Ocean.

Meyers (1980) investigated the meridional transport of the North Equatorial Countercurrent (NECC) in the Pacific Ocean and found significant inconsistency with the Sverdrup theory. Hautala et al. (1994) estimated the meridional transport of the North

* Supported by the National Basic Research Program of China (973 Program) (No. 2012CB956000) and the National Natural Science Foundation of China (Nos. 40888001, 41176019). Z. Zhang is supported by KLOCAW 1208
** Corresponding author: dyuan@qdio.ac.cn

Pacific subtropical gyre along 24°N and noted that the Sverdrup balance was invalid in the northwestern subtropical Pacific Ocean. None of these studies investigated the causes of the inconsistency.

All the existing evaluations of the Sverdrup balance have been based on one-time hydrographic measurements in a cross-basin section and have not been able to evaluate the accuracy of the theory in an integrated meridional transport from the eastern boundary. More recently, Wunsch (2011) evaluated the accuracy of the Sverdrup theory in an assimilated global ocean dataset, but a point-wise evaluation of the Sverdrup balance in the real ocean is needed. However, this evaluation has not yet been conducted because of the sparse and uneven distribution of hydrographic casts in time and space for the world's oceans, which would inevitably lead to significant aliasing errors in the mean circulation and meridional transport.

The Array for Real-time Geostrophic Observations (Argo) project has ushered in an unprecedented era of sampling the world's oceans with synchrony at basin and global scales. In this study, we calculated the absolute geostrophic currents in the North Pacific Ocean based on newly gridded Argo profiling float data. The meridional transport of the geostrophic currents was then compared with the wind-driven Sverdrup transport to evaluate the accuracy of the Sverdrup theory.

## 2 DATA AND METHOD

### 2.1 Data

The Argo data used in this study were downloaded from the website http://www.argo.ucsd.edu/Gridded_fields.html, and included salinity and temperature data on a 1°×1° horizontal grid and at 58 vertical levels. In addition, monthly climatological data were used from the Ocean General Circulation Model for the Earth Simulator (OFES), averaged from the last 10-year simulation of a 50-year model spin-up forced by the climatological National Centers for Environmental Prediction/National Center for Environmental Research (NCEP/NCAR) reanalysis data. The model domain of the OFES covers the global ocean from 75°S to 75°N, with a horizontal resolution of 0.1° longitude ×0.1° latitude and stretched vertical coordinates at 54 levels from the sea surface (2.5 m) to a maximum depth of 6 065 m. We used both the NCEP/NCAR reanalysis winds and the EAR-40 winds from the European Center for Medium-range Weather Forecasts to calculate the Sverdrup transport in this study. Satellite altimeter data from the AVISO ftp site (ftp://ftp.cls.fr) and Tropical Atmosphere-Ocean/Triangle Trans-Ocean Buoy Network (TAO/TRITON) data from the TAO website (http://www.pmel.noaa.gov/tao/) were compared with the absolute geostrophic currents based on the P-vector method (Chu, 1995).

### 2.2 P-vector method for geostrophic current calculation

The absolute geostrophic currents in this study were calculated from gridded temperature and salinity data using the P-vector method, which is based on the conservation of potential density and potential vorticity under two approximations, the geostrophic balance and the Boussinesq approximation (Chu, 1995, 2006). The intersections of isopycnic surfaces and equal-potential-vorticity surfaces determine the direction of geostrophic currents, and this direction is known as the P-vector. The thermal wind relation can be used to calculate the magnitudes of geostrophic currents at any two levels. In practice, geostrophic currents are determined by least-square fitting to the data at multiple levels. Studies have shown that the P-vector method can capture the main features of the ocean circulation in open oceans and in marginal seas (Chu, 1995, 2000; Chu et al., 1998, 2001).

In previous studies (e.g. Chu, 1995), P-vector geostrophic currents were calculated by applying least-square fitting to the entire ocean column. However, motion in the upper mixed layer of the ocean does not generally conform to the conservation of density and potential vorticity. Therefore, in this study we chose to construct the geostrophic currents only in the intermediate layers and the P-vector method was used to calculate the geostrophic currents between 800–2 000 dbar. The geostrophic currents above 800 dbar were determined by dynamic calculation, using geostrophic currents at 800 dbar as the reference velocity.

Previous analyses have shown that absolute geostrophic currents are not sensitive to the choice of depth ranges as long as the P-vector calculation is conducted well below the surface mixed layer. Calculated geostrophic currents have captured the main features of the North Pacific Ocean circulation including the North Equatorial Current (NEC), the NECC, the Subtropical Countercurrent (STCC), and the Kuroshio extension (Fig.1). We compared the interannual variation of absolute geostrophic currents

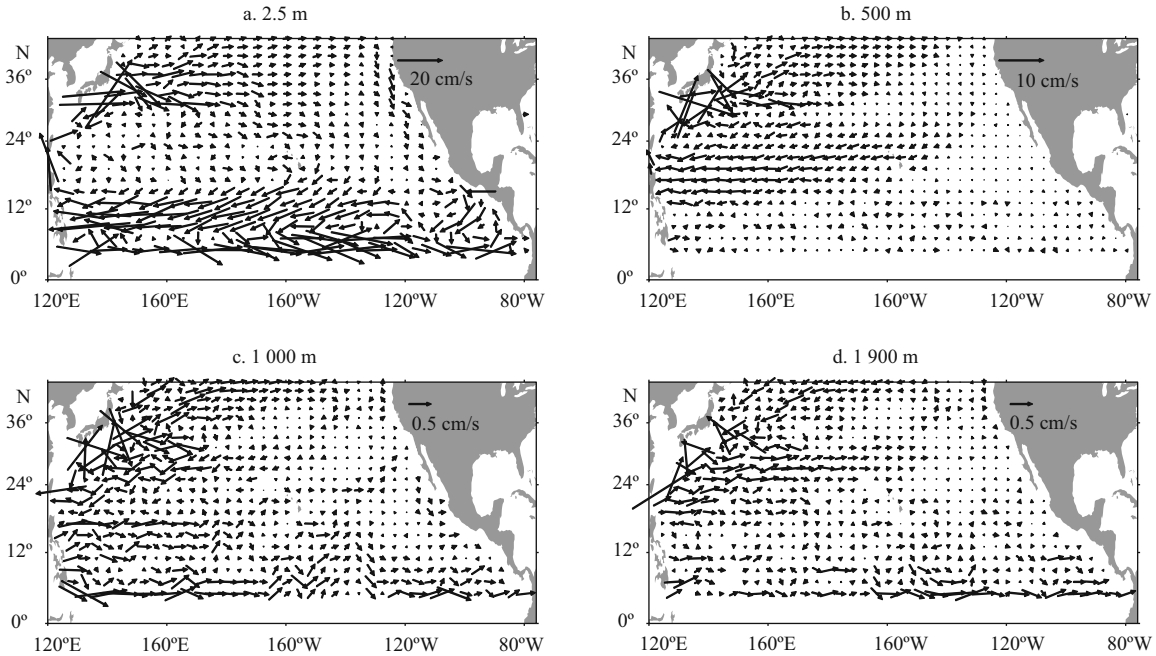


**Fig.1 Distribution of mean surface absolute geostrophic currents from 2004–2009 at different depths in the North Pacific Ocean**

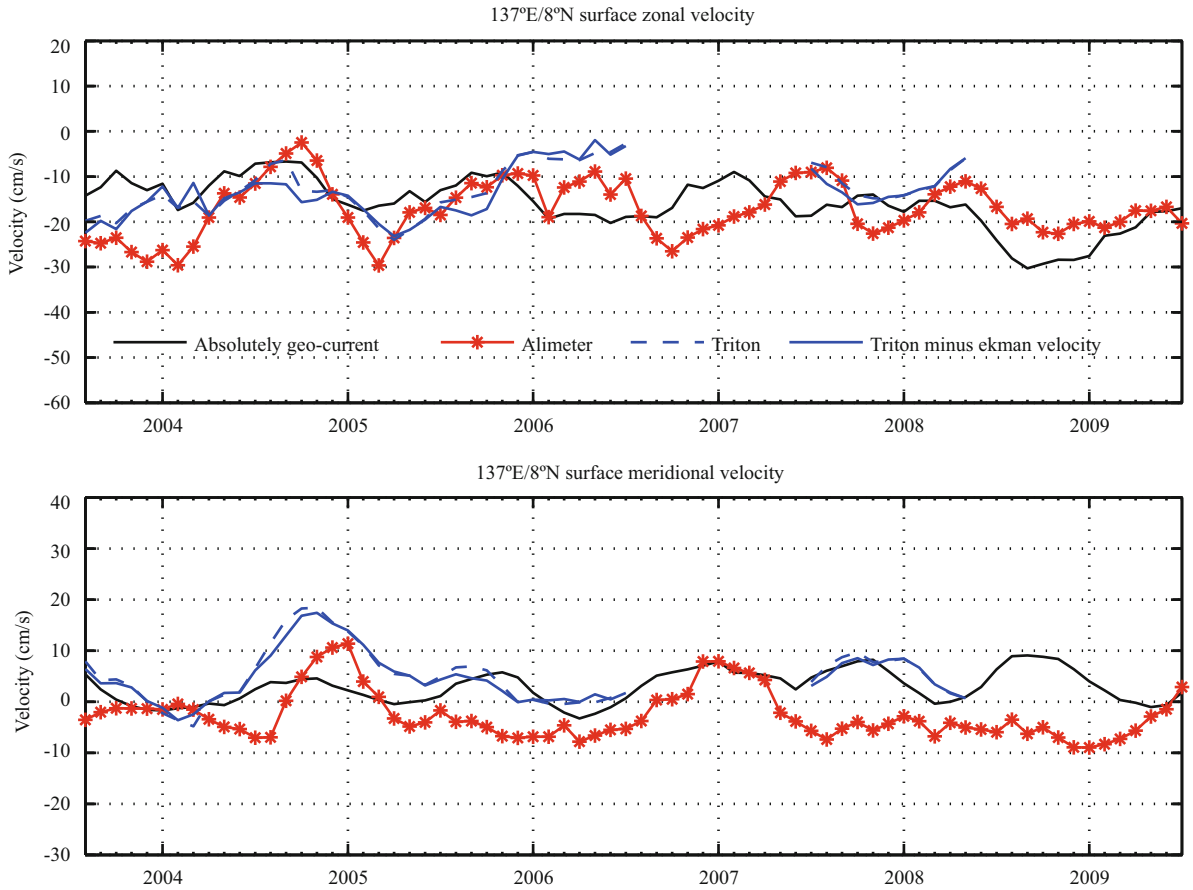


**Fig.2 Comparison of currents at a depth of 10 m at 137°E, 8°N, from 2004–2009**

Absolute geostrophic currents reconstructed using the P-vector method (black solid line), the in-situ TRITON data with the Ekman velocity subtracted (blue solid line), the in-situ TRITON data (blue dashed line), and the satellite altimeter surface geostrophic currents (red solid line). The upper panel is zonal velocity, and the lower panel is meridional velocity.

with TRITON data at 137°E, 8°N (Fig.2). The interannual variation in the surface geostrophic currents based on satellite altimeter sea level is also plotted for reference. An Ekman velocity based on the monthly NCEP/NCAR winds was deducted from the TRITON moored time series measurements at 137°E, 8°N. The vertical eddy viscosity coefficient ($A_z$) was assumed to be 0.012 $m^2/s$, corresponding to an Ekman layer depth ($D$) of about 91 m. The comparison showed good agreement, with correlations between the P-vector geostrophic currents and the TRITON current meter measurement of 0.605 06 and 0.669 64 for the zonal and meridional velocity components, respectively (Fig.2). The correlations between the altimeter geostrophic currents and the TRITON measurements were 0.700 87 and 0.797 4 in the zonal and meridional directions, respectively. The comparisons were not sensitive to the value of the vertical eddy viscosity, because the Ekman layer depth was much greater than the depth of the current meter, supporting the accuracy of the absolute geostrophic currents.

Errors in absolute geostrophic currents are made up of two components; one estimated based on the standard deviation of the absolute geostrophic currents themselves and the other estimated based on the thermal wind relation with the variability in Argo density measurements. The meridional transport error can then be obtained by vertically integrating the meridional velocity error from top (2.5 m) to bottom (1 900 m) in each grid.

### 2.3 The Sverdrup balance

The Sverdrup theory suggests that the total meridional transport of the mean ocean circulation can be determined by surface wind-stress curl forcing (Sverdrup, 1947). The theory can be demonstrated conveniently using a vertical integration of the steady state vorticity balance:

$$\beta v = f \frac{\partial w}{\partial z}, \tag{1}$$

where $v$ is the meridional component of the geostrophic velocity, $w$ is the vertical velocity component, $f$ is the Coriolis parameter, and $\beta = \mathrm{d}f/\mathrm{d}y$ is the meridional gradient of the Coriolis parameter related to the curvature of the Earth's surface. The meridional transport from the surface to depth ($-H$) along latitude ($y$) from the eastern boundary ($x_E$) to longitude ($x$) can be calculated according to Hautala et al. (1994):

$$\frac{1}{\rho_0}\int_{x_E}^{x}\int_{-H}^{0}\rho v\,\mathrm{d}z\mathrm{d}x = \frac{1}{\beta\rho_0}\int_{x_E}^{x}\mathbf{k}\cdot(\nabla\times\boldsymbol{\tau})\,\mathrm{d}x + \frac{1}{f\rho_0}\int_{x_E}^{x}\tau^x\mathrm{d}x, \tag{2}$$

where $\rho$ is the water density, $\rho_0$ (=1 025 $kg/m^3$) is the characteristic water density, $\mathbf{k}$ is the unit vector in the vertical direction (upward positive), $\boldsymbol{\tau}$ is the wind stress vector $\boldsymbol{\tau}=(\tau^x, \tau^y)$, and $x_E$ and $x$ are the eastern boundary and the western end points of the integration, respectively. The vertical velocity $w$ is assumed to vanish at the depth $z=-H$, where $H$ is set at 1 900 m or a specified isopycnal (see below). Both sides of Eq.2 vary with ($x$, $y$). The left side is the geostrophic meridional transport (calculated from ocean hydrographic data) and the right side is the wind-driven Sverdrup meridional transport (computed from surface wind stress). The traditional Sverdrup transport includes the geostrophic transport and the Ekman meridional transport determined by wind curl forcing according to Eq.2.

## 3 RESULT

### 3.1 Discrepancy of geostrophic transport from the Sverdrup relation

The North Pacific Ocean was chosen to assess the validity of the Sverdrup relation (Eq.2) in this study. The mean geostrophic meridional transport (Fig.3a) and the wind-driven Sverdrup meridional transport (Fig.3b) in the North Pacific for the period 2004–2009 were calculated based on the left and right sides of Eq.2. The gridded ($T$, $S$) fields from Argo profiles averaged over 2004–2009 were used with the P-vector method to calculate the geostrophic meridional transport. The NCEP surface wind stress ($\boldsymbol{\tau}$) data averaged over the years 2004–2009 were used to compute the wind-driven Sverdrup meridional transport. The wind-driven Sverdrup meridional transport was subtracted from the geostrophic meridional transport to yield the meridional transport discrepancy shown in Fig.3c. The wind-driven Sverdrup meridional transport was generally in good agreement with the geostrophic meridional transport in the eastern subtropical Northwest Pacific Ocean and in the areas along 12°–15°N and 21°–27°N west of the dateline.

The agreement of the wind-driven Sverdrup meridional transport with the geostrophic meridional transport in the area from 21°–27°N is consistent with the findings of Hautala et al. (1994) along 24°N.

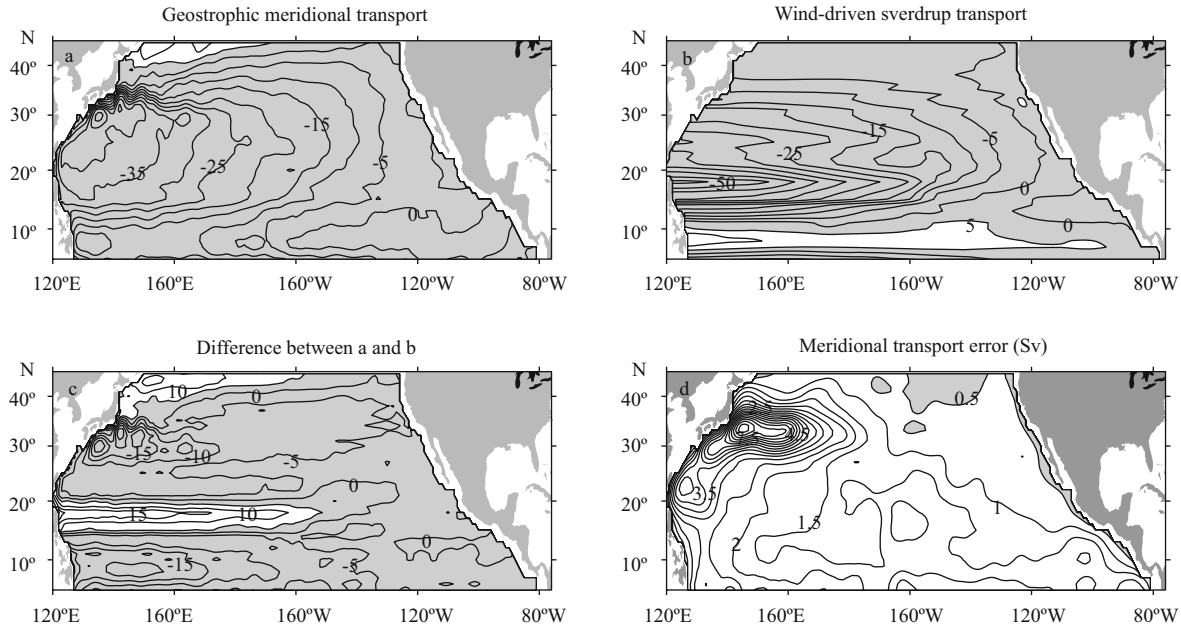


**Fig.3 a. Geostrophic meridional transport calculated from mean (2004–2009) Argo (*T*, *S*) profiles using the P-vector method; b. Wind-driven Sverdrup meridional transport from the annual mean (2004–2009) NCEP surface wind stress; c. Meridional transport discrepancy (geostrophic minus wind-driven meridional transport) over the North Pacific (contour interval is 5 Sv); d. Grid error estimate of the geostrophic meridional transport over the North Pacific Ocean (contour interval is 0.5 Sv)**

However, the wind-driven meridional transport failed to explain the geostrophic meridional transport in the recirculation and the extension regions of the Kuroshio, as a result of the linear approximation in the Sverdrup theory.

Significant differences between the geostrophic meridional transport and the wind-driven Sverdrup meridional transport were also found for 6°–12°N, 140°E–140°W, between the NEC and the NECC, and for 15°–20°N, 140°E–120°W, between the NEC and STCC, as shown in Fig.3c. The maximum differences were larger than 20 Sv (1 Sv=$10^6$ $m^3/s$), much larger than the error estimate of the transport shown in Fig.3d, suggesting that the deviation was significant and that surface wind curl is not the only factor forcing ocean circulations. In particular, the wind-driven Sverdrup meridional transport and the geostrophic meridional transport have opposite signs in the region between 6°–12°N in the western Pacific Ocean, showing that the geostrophic currents there are not governed solely by wind-stress curl forcing.

Godfrey (1989), Qiu and Joyce (1992), and Hautala et al. (1994) have suggested that the wind-driven meridional transport is dependent on wind products and drag coefficients. Meyers (1980) suggested that the drag coefficients contribute about 20% inaccuracy to the estimation of the wind-driven Sverdrup meridional transport. The uncertainty in the wind-stress is clearly responsible for the meridional transport discrepancy in the interior tropical and subtropical Northwest Pacific Ocean calculated from the Sverdrup balance. However, the significant difference between the geostrophic meridional transport and the wind-driven Sverdrup meridional transport is robust for different wind products and different drag coefficients, and is independent of the depth range of the vertical integration (see below).

### 3.2 Independence of meridional transport discrepancy on depth *H*

The Sverdrup relation (Eq.2) is established with the assumption of zero vertical velocity at the depth $z=-H$, where $H$=1 900 m in Section 3.1. Many earlier discussions about the Sverdrup balance have been based on the assumption that the abyssal and bottom vertical velocity are negligible (Marchuk et al., 1973). Marchuk et al. (1973) believed that the assumption of zero vertical velocity at the depth $z=-H$ (where $H$ is constant, not a function of $X$ and $Y$) is one of the principal restrictions of the Sverdrup theory. The effect of the baroclinic nature of large-scale ocean circulation and bottom relief is crucial to observed peculiarities in steady large-scale currents in the

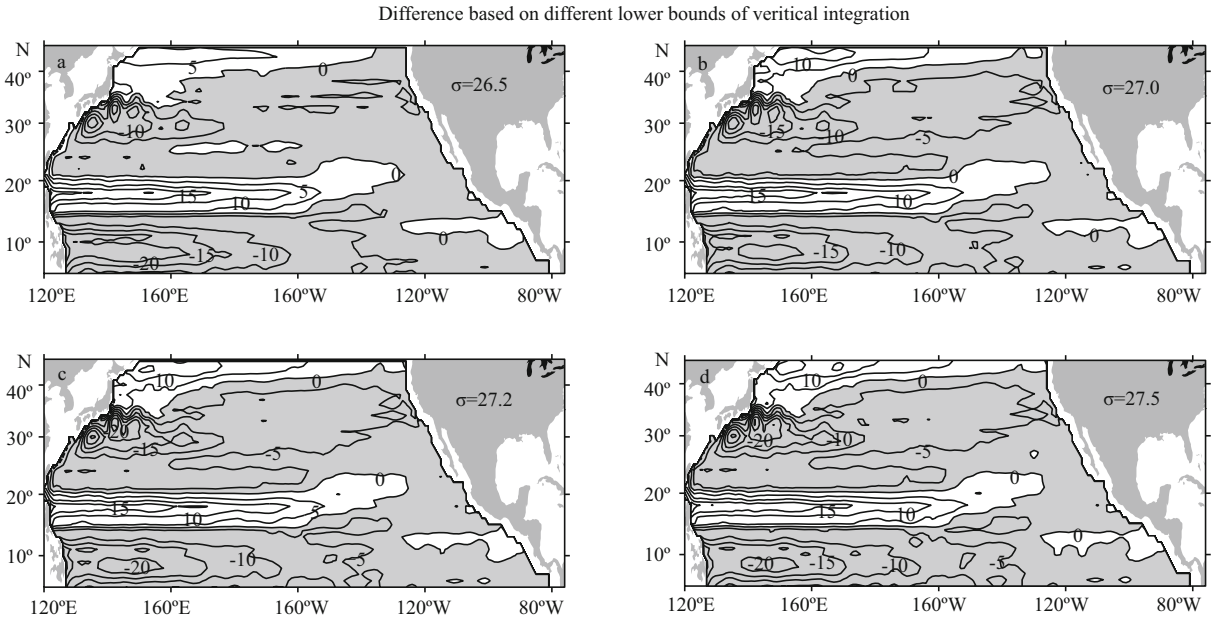


**Fig.4 Dependence of the meridional transport discrepancy on the choice of the isopycnic surfaces of (a) 26.5$\sigma_\theta$, (b) 27$\sigma_\theta$, (c) 27.2$\sigma_\theta$, and (d) 27.5$\sigma_\theta$, as the bottom limits of the integration (contour interval is 5 Sv)**

world's oceans. So far, no theory has predicted the value of $z$, if it exists, although some parameters have been selected and used in the literature, including fixed depths and isopycnals. However, none of the standard parameters selected can be justified, or can be expected to be globally applicable. To test the sensitivity of meridional transport discrepancy to the selection of $H$, the meridional transport difference between the left and right sides of Eq.2 was calculated with different values of $H$ (corresponding to isopycnal of 26.5$\sigma_\theta$, 27.0$\sigma_\theta$, 27.2$\sigma_\theta$, and 27.5$\sigma_\theta$) for the left side of the equation, as shown in Fig.4. The overall structure of the meridional transport discrepancy for different $\sigma_\theta$ levels is similar to that in Fig.1c. The deviations of the geostrophic meridional transport from the wind-driven Sverdrup meridional transport in the areas 6°–12°N and 15°–20°N were significant and evidently independent of the bottom limits of the geostrophic meridional transport integration.

### 3.3 Independence of meridional transport discrepancy on surface wind data

We conducted a further analysis to investigate the reason for the large difference between the geostrophic meridional transport from the Sverdrup linear theory in the areas 6°–12°N and 15°–20°N in the western North Pacific. Averaged ERA-40 surface wind data for the period 1961–2000 and averaged NCEP/NCAR reanalysis surface wind data for 1948–2009 were used to examine the sensitivity of the meridional transport discrepancy to the surface wind products. These surface wind-stress products were estimated using the drag coefficient described by Large and Pond (1981) shown in Eq.4 below.

The differences between the left and the right sides of Eq.2 for the different wind products are shown in Fig.5a and 5b. For these experiments, the lower limit of the vertical integration of the geostrophic meridional transport was set at $\sigma_\theta$=27.2. The spatial patterns of the deviation from the Sverdrup theory in Fig.5a and 5b for the different wind products were similar to those in Fig.3c, with the maximum differences larger than 20 Sv, suggesting that the deviation from the Sverdrup theory in these two areas is robust.

For the region between 15°–20°N, the two experiments showed somewhat different results. The southward meridional transport calculated from the long-term (1948–2009) averaged NCEP wind stress data was about 5 Sv more than that calculated from the short-term (2004–2009) averaged NCEP wind stress data, resulting in about 5 Sv less in meridional transport discrepancy in Fig.5b than in Fig.3c. The discrepancy from the ERA wind-forced meridional transport in this area was even less in Fig.5a than in Fig.3c, but the negative difference north of the Kuroshio recirculation area was significantly larger

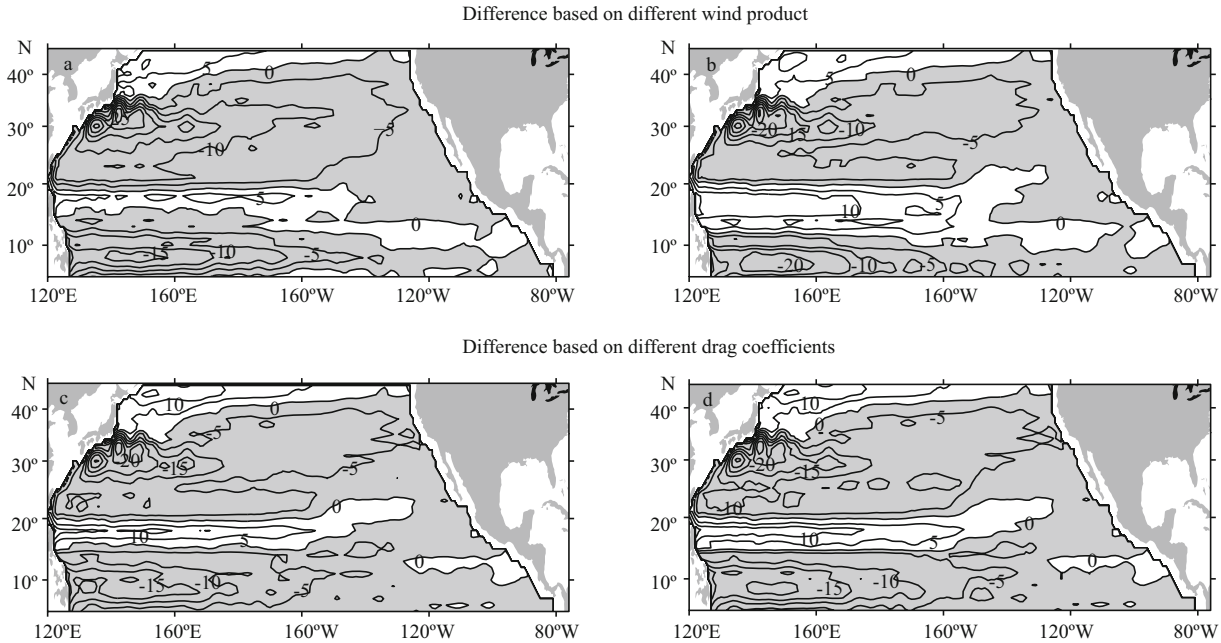


**Fig.5 Meridional transport discrepancy based on (a) ERA-40 surface mean (1961–2000) wind stress, (b) NCEP surface mean (1948–2009) wind stress, (c) NCEP surface mean (2004–2009) wind vector using the Large and Pond (1981) drag coefficients, and (d) NCEP surface mean (2004–2009) wind vector using the Foreman and Emeis (2010) drag coefficients**

than that in Fig.5a. These results suggest that wind stress errors do not account for all of the meridional transport discrepancies from the Sverdrup theory.

### 3.4 Independence of meridional transport discrepancy on drag coefficients

For a given surface wind vector $\mathbf{u}=(u, v)$, the wind stress vector $\boldsymbol{\tau}$ is calculated by the drag law:

$$\boldsymbol{\tau} = \rho_a C_d |\mathbf{u}| \mathbf{u} , \quad (3)$$

where $\rho_a$ is the air density at the sea surface, and $C_d$ is the drag coefficient, which is determined empirically by the observational data. For example, Large and Pond (1981) proposed the following formula for the drag coefficient:

$$C_d = \begin{cases} 1.2\times10^{-3}, & |\mathbf{u}| < 11 \text{ m/s} \\ (0.49+0.065|\mathbf{u}|)\times10^{-3}, & |\mathbf{u}| > 11 \text{ m/s} \end{cases} . \quad (4)$$

The Large and Pond (1981) formula (Eq.4) shows that the drag coefficient increases with wind speed. Recent studies indicate that the drag coefficient in the marine atmospheric boundary layer does increase with wind speed for moderate winds, but levels out at high wind speeds (Foreman and Emeis, 2010). To analyze the sensitivity of the meridional transport discrepancy to the drag coefficient ($C_d$), a formula proposed recently by Foreman and Emeis (2010) for wind speed less than 30 m/s was used:

$$C_d = \begin{cases} 1.139\times10^{-3}, & |\mathbf{u}| < 8 \text{ m/s} \\ \dfrac{\left[-0.000018|\mathbf{u}|^2 + 0.051(|\mathbf{u}|-8) + 0.27\right]^2}{|\mathbf{u}|^2}, & |\mathbf{u}| > 8 \text{ m/s} \end{cases} . \quad (5)$$

The use of the Foreman and Emeis (2010) drag coefficients resulted in a similar pattern for the geostrophic meridional transport discrepancies from the wind-driven Sverdrup meridional transport as in Fig.3c. The magnitudes of the meridional transport discrepancies using the Foreman and Emeis (2010) drag coefficients in Fig.5d are about 5 Sv larger than those generated using the Large and Pond (1981) drag coefficients shown in Fig.5c. This suggests that uncertainty in the drag coefficients is not the primary reason for the geostrophic meridional transport discrepancies from the wind-driven Sverdrup meridional transport.

### 3.5 Nonlinear effects of ocean circulation

The high-resolution OFES model provides an opportunity to investigate the origin of the meridional transport discrepancy in the interior tropical and subtropical Northwest Pacific Ocean. The climatological annual mean NCEP winds, the OFES ($T$, $S$), and velocity fields were used for this investigation. The wind-driven Sverdrup meridional transport was estimated based on the climatological annual mean NCEP surface wind stress for 1996–

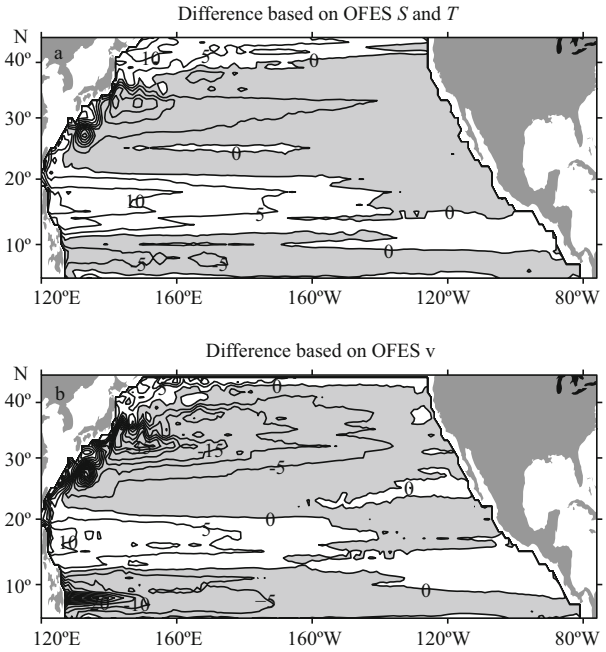


**Fig.6 Meridional transport discrepancy with geostrophic currents (a) calculated from the OFES simulated (*T*, *S*) field using the P-vector method (type-1 meridional transport discrepancy); (b) meridional transport discrepancy between the total meridional transport of the OFES simulation with the Ekman transport subtracted and the wind-driven Sverdrup meridional transport (type-2 meridional transport discrepancy)**

2006 using the drag coefficient from Eq.4. The geostrophic meridional transport was calculated from the OFES climatological annual mean (*T*, *S*) simulation using the P-vector method. The lower boundary for the vertical integration (*H*) was chosen as 1 900 m. Experiments using different isopycnic surfaces ($26.5\sigma_\theta$, $27\sigma_\theta$, $27.2\sigma_\theta$ and $27.5\sigma_\theta$) as the lower boundary of the vertical integration of the geostrophic meridional transport calculation showed essentially the same results (not shown). Figure 6a shows the significant meridional transport discrepancy (type-1) in the latitudinal bands of 6°–12°N and 12°–20°N, the magnitude and area coverage being essentially the same as those based on the Argo data (Fig.3c). The maximum differences are ~10 Sv in region of 6°–12°N and more than 20 Sv in region of 12°–20°N. The OFES simulation is dynamically consistent with the wind forcing therefore the Sverdrup balance would be satisfied if the dynamics were linear. The above comparison strongly suggests that the significant meridional transport discrepancy is a result of nonlinear effects of the OFES model.

An alternative method for calculating the ocean total meridional transport is to use the OFES velocity output (i.e., geostrophic plus ageostrophic velocity). Subtracting the meridional Ekman transport:

$$\mathrm{MVT}_{\mathrm{Ekman}} = -\frac{1}{f\rho_0}\int_{x_E}^{x}\tau^x \mathrm{d}x\,, \tag{6}$$

from the total meridional transport leads to the interior meridional transport. Then the meridional transport discrepancy from the wind-driven Sverdrup meridional transport (type-2 meridional transport discrepancy) is calculated, as shown in Fig.6b. The type-2 meridional transport discrepancy is essentially the same as type-1 (Fig.6a) in the interior tropical Northwest Pacific Ocean, which suggests that the geostrophic current is a valid approximation of the leading order general ocean circulation in the North Pacific Ocean. In the areas east of Mindanao and east of Japan, the discrepancy suggests that the ageostrophic component becomes important in areas where the type-2 meridional transport is larger than the type-1 discrepancy. The similar patterns of the meridional transport discrepancies of both types suggest that the identified deviation from the Sverdrup linear dynamics should be robust.

## 4 CONCLUSION

In this study, absolute geostrophic currents in the North Pacific Ocean were calculated based on the gridded Argo profiling float data for the period from January 2004 to December 2009, using the P-vector method. The meridional transport of the geostrophic currents was compared with the wind-driven Sverdrup meridional transport in the North Pacific Ocean to assess the accuracy of the Sverdrup theory. The results showed large differences from the Sverdrup balance in the regions 6°–12°N, and 15°–20°N, and in the recirculation and extension areas of the Kuroshio in the Northwest Pacific Ocean. Analyses suggest that although large uncertainties exist in the wind stress estimates, the robust patterns of the deviation from the Sverdrup balance indicate that wind stress errors are not the primary cause of the large differences. A comparison of the geostrophic meridional transport and the wind-driven Sverdrup meridional transport in the high-resolution OFES simulation showed a similar difference. It is suggested that the nonlinear effects of the ocean circulation are the most likely cause of the differences. The results of this study suggest that the linear dynamics of the Sverdrup theory are too simple to explain the meridional transport in the tropical Northwest Pacific Ocean.

## 5 ACKNOWLEDGEMENT

We are very thankful to two anonymous reviewers for helpful comments.

**References**

Böning C W, Döscher R, Isemer H J. 1991. Monthly mean wind stress and Sverdrup transports in the North Atlantic: a comparison of the Hellerman-Rosenstein and Isemer-Hasse Climatologies. *J. Phys. Oceanogr.*, **21**(2): 221-235.

Chu P C. 1995. P-vector method for determining absolute velocity from hydrographic data. *Marine Tech. Soc. J.*, **29**(2): 3-14.

Chu P C. 2000. P-vector spiral and determination of absolute velocities. *J. Oceanogr.*, **56**: 591-599.

Chu P C. 2006. P-Vector Inverse Method. Springer. 605pp.

Chu P C, Fan C W, Lozano C J, Kerling J. 1998. An airborne expandable bathythermograph (AXBT) survey of the South China Sea, May 1995. *J. Geophys. Res.*, **103**: 21 637-21 652.

Chu P C, Lan J, Fan C W. 2001. Japan Sea circulation and thermohaline structure Part I, Climatology. *J. Phys. Oceanogr.*, **31**: 244-271.

Foreman R J, Emeis S. 2010. Revisiting the definition of the drag coefficient in the marine atmospheric boundary layer. *J. Phys. Oceanogr.*, **40**: 2 325-2 332.

Godfrey J S. 1989. A Sverdrup model of the depth-integrated flow for the world ocean allowing for island circulations. *Geophys. Astrophys. Fluid Dyn.*, **45**: 89-112.

Hautala S L, Roemmich D H, Schmitz Jr W J. 1994. Is the North Pacific in Sverdrup balance along 24°N? *J. Geophys. Res.*, **99**: 16 041-16 052.

Large W G, Pond S. 1981. Open ocean momentum flux measurements in moderate to strong wind. *J. Phys. Oceanogr.*, **11**: 324-336.

Leetmaa A, Niiler P, Stommel H. 1977. Does the Sverdrup relation account for the mid-Atlantic circulation? *J. Mar. Res.*, **35**: 1-10.

Meyers G. 1980. Do Sverdrup transports account for the Pacific North Equatorial Countercurrent? *J. Geophys. Res.*, **85**(2): 1 073-1 075.

Marchuk G I, Sarkisian A J, Kochergin V P. 1973. Calculations of flows in a baroclinic ocean: numerical methods and results. *Geophysical and Astrophysical Fluid Dynamics*, **5**(1): 89-99.

Qiu B, Joyce T M. 1992. Interannual variability in the mid- and low-latitude western North Pacific. *J. Phys. Oceanogr.*, **22**: 1 062-1 079.

Schmitz Jr W J, Thompson J D, Luyten J R. 1992. The Sverdrup circulation for the Atlantic along 24°N. *J. Geophys. Res.*, **97**(5): 7 251-7 256.

Sverdrup H U. 1947. Wind-driver currents in a baroclinic ocean; with application to the equatorial current of the eastern Pacific. *Proc. Natl. Acad. Sci.*, **33**: 318-326.

Wunsch C. 2011. The decadal mean ocean circulation and Sverdrup balance. *J. Mar. Res.*, **69**: 417-434.

Wunsch C, Roemmich D. 1985. Is the North Atlantic in Sverdrup balance? *J. Phys. Oceanogr.*, **15**: 1 876-1 880.